Pergamon

Solid-State Electronics Vol. 42, No. 3, pp. 453–457, 1998

Printed in Great Britain
0038-1101/98 $19.00 + 0.00

NOTE

A MODEL FOR LOW-TEMPERATURE OPERATION OF MINORITY-CARRIER WELL-TYPE GUARD RINGS IN EPITAXIAL CMOS STRUCTURES††

(Received 12 December 1996; in revised form 19 June 1997)

Abstract As temperature is lowered, behaviors of well-type guard rings in an epitaxial substrate are quite different from those at RT so that the previous formulation is unable to reflect these discrepancies precisely. This leads to a new escape-current model suitable for low-temperature applications. In addition to the structural parameters, the new model is also functions of other physical quantities such as temperature, high-level injection, surface recombination velocity at the high/low junction and minority-carrier transport parameters, which are also important at low temperature. © 1997 Elsevier Science Ltd

1. INTRODUCTION

Minority-carrier well-type guard ring is one of the most effective layout techniques for latch-up prevention in CMOS structures[1,2]. The well-type guard rings surrounding the parasitic minority-carrier injectors in the I/O region were utilized to collect the minority carriers injected into the substrate, and thus to avoid latchup. The efficiency of such guard rings can be enhanced greatly by an epitaxial layer grown on a heavily-doped substrate[3,4]. The escape current composed of minority carriers escaping from the guard-ring collection can be divided into the sandwich and substrate components[5,6]. Based on this result an analytic design model was proposed and also used to establish design guidelines for minimum area consumption[5–7]. This provides a fast means of calculation for guard ring structure design. In contrast, the collection efficiency variation and stronger width dependence of the guard rings operated at 77 K were also reported[8]. As temperature is lowered, the escape current characteristics and their mechanisms are far from those at RT. Although the model developed at RT can still be applied to the escape-current characteristics at low temperature, its fitness becomes a purely empirical process. Therefore, in this work, a new escape-current model based on the new physical assumptions at low temperatures is derived to quantitatively describe the behaviors and to give physical insights for low-temperature operation. This new model may give an efficient approach to evaluate and analyze the guard-ring structures without a large number of numerical simulations.

2. MODEL DEVELOPMENT

Figure 1 shows schematically the right-hand-side cross-sectional view of an n-well guard ring structure on an epitaxial substrate. The fabrication details of this structure were mentioned in [7]. According to the previous reports[5,6], the escape current can be divided into two components: the first caused by minority carriers injected into a sandwich layer between the upper collecting plate and the bottom reflecting plate, namely sandwich escape current I_{san}, and the second caused by those penetrating the epitaxial high/low junction and then spreading out in the large, highly-doped substrate, namely substrate escape current I_{sub}. Such division viewpoint is still feasible at low temperatures. As for the I_{sub} component, the basic form, in which the parameters are determined empirically, are all the same at low temperatures without any further modification. Therefore the following discussions will concentrate on the usually dominant and important component, i.e., the I_{san} component.

According to the previous report on the low-temperature operations[8], the mechanisms and properties of the escape current are quite different from those at RT. The different conditions from those at RT are as follows.

(i) High-level injection phenomenon becomes severe in most part of the structure and the extension of the depletion region covering the sandwich layer depends on injection level, temperature, and the structural dimensions in the devices. The original minority carrier diffusion equation was changed to $\nabla^2 n(x, y) - n(x, y)/\xi L_{nl}^2 = 0$, in which complicated behavior can be simply accounted for by a high injection parameter ξ. $\xi = 1$ represents the ordinary low-level injection and $\xi = 2$ represents the extremely high injection condition[4,9]. In the equation $n(x, y)$ is the injected excess minority-carrier density and L_{nl} is the minority-carrier diffusion length in the sandwich layer.

(ii) The surface recombination velocity of the minority carriers at the high/low junction becomes significant, and must be included in the boundary conditions at low temperature. Its analytic expression should also be derived in order to give full physical meaning.

(iii) The boundary at the bottom edge of the depletion region across the n-well was changed to the metallurgical junction depth x_j of the well because of the arbitrary extension of the depletion region. These new circumstances thus lead to the modified boundary conditions as shown in Fig. 2.

(i) The excess minority-carrier concentration $n(x, y) = 0$ at $x = x_j$ owing to the ideal assumption that the minority carriers are infinitely absorbed by the well. Irrespective of such simplified boundary condition, the resulting model was confirmed favorably as will be shown later.

†This work was supported by the National Science Council under Contract NSC 84-2215-E-009-043.

(ii) The large surface recombination at the high/low junction makes the boundary condition at $x = x_e^-$ as $-J_n|_{x=x_e^-} = qS_{pp^+}(n(x_e^-, y) - n_0)$[9].

(iii) $n(x, y)$ becomes zero for $y \to \infty$ because the right hand side of the sandwich layer is far in distance from the injection side; (iv) the concentration at $y = y_2$, the injection side of the sandwich layer, is assumed to be a specific $n(x, y_2)$ subject to injection condition of the lateral bipolar structure besides the sandwich layer. The corresponding diffusion equation in the sandwich region of $x_j \leqslant x \leqslant x_e$ and $y_2 \leqslant y$ in Fig. 2 is given by $\nabla^2 n(x, y) - n(x, y)/\xi L_{nl}^2 = 0$ as mentioned before. By the separation of variables, the solution has the following general form;

$$n(x, y) = A \cdot \sin(m(x - x_j)) \cdot \exp\left(-\sqrt{\frac{1}{\xi L_{nl}^2} + m^2}(y - y_2)\right) \quad (1)$$

For $m(x_e - x_j)$ close to $\pi/2$, $\cot(m(x_e - x_j))$ can be approximated by

$$\frac{1}{m(x_e - x_j)} - \frac{m(x_e - x_j)}{3},$$

which is the first two terms of the $\cot(m(x_e - x_j))$ infinite series. Therefore m is solved to be;

$$m = \frac{2n\pi}{(x_e - x_j)} + \frac{1}{(x_e - x_j)}\sqrt{3\left(1 + \frac{S_{pp^+}}{\xi D_{nl}}(x_e - x_j)\right)} \quad n = 0, 1, 2, \ldots \quad (3)$$

and the total solution becomes;

$$n(x, y) = \sum_{n=0}^{\infty} A_n \cdot \sin\left(\left(\frac{2n\pi}{(x_e - x_j)} + \frac{1}{(x_e - x_j)}\sqrt{3\left(1 + \frac{S_{pp^+}}{\xi D_{nl}}(x_e - x_j)\right)}\right)(x - x_j)\right) \cdot \exp\left(-\sqrt{\frac{1}{\xi L_{nl}^2} + \left(\frac{2n\pi}{(x_e - x_j)} + \frac{1}{(x_e - x_j)}\sqrt{3\left(1 + \frac{S_{pp^+}}{\xi D_{nl}}(x_e - x_j)\right)}\right)^2}(y - y_2)\right) \quad (4)$$

where A and m are two coefficients to be determined. Next the boundary condition at $x = x_e^-$, i.e., $-J_n|_{x=x_e^-} = qS_{pp^+}(n(x_e^-, y) - n_0)$ is applied to finding the m coefficient, and we have;

$$m \cdot \cot(m(x_e - x_j)) = -\frac{S_{pp^+}}{\xi D_{nl}} \quad (2)$$

Normally

$$\frac{1}{\sqrt{\xi L_{nl}}} \ll \frac{2n\pi}{(x_e - x_j)} + \frac{1}{(x_e - x_j)} \times \sqrt{3\left(1 + \frac{S_{pp^+}}{\xi D_{nl}}(x_e - x_j)\right)}.$$

This is because the diffusion constant $L_{nl} \gg (x_e - x_j)$[10] and the numerator of the right-hand side is larger than 1. The solution is a rapidly decreasing exponential function of y, so only the first term of the general solution is retained. Its coefficient A_0 is determined by the final boundary condition at the injection side of the sandwich layer. It not only depends on the gain of the lateral bipolar transistor, but also on the 2-D geometry around the injection side of the sandwich layer. The ordinary formulation of the minority carrier concentration cannot apply to this quantity. It is a complex function of the 2-D geometrical dimensions around the sandwich layer, emitter–substrate bias and doping profiles of the lateral bipolar transistor, and a fully

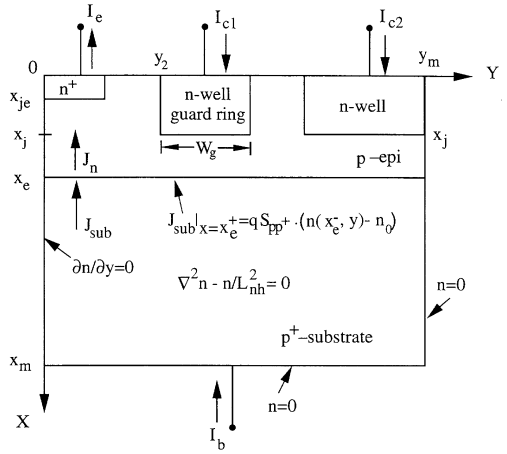

Fig. 1. The schematic cross-sectional view of the n-well guard-ring structure on the p-epi/p^+-substrate where the n^+ emitter, n^+ collector and outer n-well collector are also shown. Also shown in the figure is the boundary value problem for analytically solving the surface recombination velocity S_{pp^+} at the high/low junction, x_m and y_m are located at the bottom metal contact and the right side of the structure, and J_{sub} is the minority-carrier current in the heavily-doped substrate.

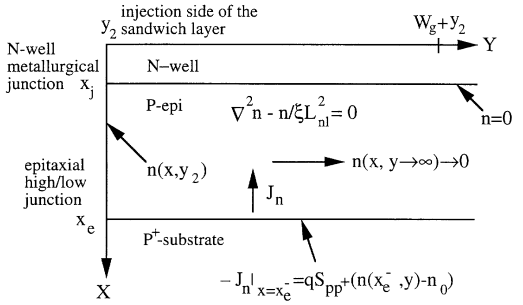

Fig. 2. The boundary value problem for solving the I_{san} component of the escape current. y_2 is the location of the guard ring edge facing the n^+ emitter, x_j is the n-well metallurgical junction depth and x_e is the epitaxial high/low junction depth.

analytical solution would become too complex to use. For the sake of simplicity we just treat A_0 as a fitting parameter n^* and this will not harm the first-order effectiveness of the model. Therefore we obtain the final solution form;

$$n(x, y) = n^* \cdot \sin\left(\sqrt{3\left(1+\frac{S_{pp^+}}{\xi D_{\mathrm{nl}}}(x_{\mathrm{e}} - x_{\mathrm{j}})\right)}\right) \times \frac{(x - x_{\mathrm{j}})}{(x_{\mathrm{e}} - x_{\mathrm{j}})}\cdot \exp\left(-\sqrt{3\left(1+\frac{S_{pp^+}}{\xi D_{\mathrm{nl}}}(x_{\mathrm{e}} - x_{\mathrm{j}})\right)}\right) \frac{(y - y_2)}{(x_{\mathrm{e}} - x_{\mathrm{j}})}\right) \quad (5)$$

and the escape current is also obtained as following;

$$I_{\mathrm{esc}} = \int_{y_2 + W_{\mathrm{g}}}^{\infty} q\xi D_{\mathrm{nl}} \cdot \left|\frac{\partial n(x, y)}{\partial x}\right|_{x = x_{\mathrm{j}}} W_{\mathrm{eff}}\, \mathrm{d}y = q\xi D_{\mathrm{nl}} W_{\mathrm{eff}} n^* \exp\left(-\sqrt{3\left(1+\frac{S_{pp^+}}{\xi D_{\mathrm{nl}}}(x_{\mathrm{e}} - x_{\mathrm{j}})\right)}\right) \frac{W_{\mathrm{g}}}{(x_{\mathrm{e}} - x_{\mathrm{j}})}\right) \quad (6)$$

W_{eff} is the effective peripheral length of the test structure. This is an equation form similar to that at RT in [5,6] with two fitting parameters ξ, n^* and L_{eff} equal to

$$\frac{(x_{\mathrm{e}} - x_{\mathrm{j}})}{\sqrt{3\left(1+\frac{S_{pp^+}}{\xi D_{\mathrm{nl}}}(x_{\mathrm{e}} - x_{\mathrm{j}})\right)}}.$$

3. DERIVATION OF THE SURFACE RECOMBINATION VELOCITY

Surface recombination velocity of the high/low junction becomes significant at low temperature. Its correlations with other physical parameters should be clarified in advance to give its full physical implication. Consider the heavily-doped substrate region as shown in Fig. 1. Along the high/low junction the boundary condition is $J_{\mathrm{sub}}|_{x = x_{\mathrm{e}}^+} = qS_{pp^+}(n(x_{\mathrm{e}}^-, y) - n_0)$[9], where the $n(x, y)$ is the minority carrier concentration to be solved. At the left edge the current flow pattern is symmetric so that only the vertical component is allowed, thus $\partial n(x, y)/\partial y = 0$. At the far right end of the structure where minority carriers were recombined and collected nearly completely, the $n(x, y)$ is assumed to be zero. The $n(x, y)$ is equal to zero at the substrate contact because of the infinite recombination velocity of the metal contact. Finally, as confirmed by the simulation results, the minority-carrier concentration becomes far less than the substrate doping concentration especially underneath the outer n-well, so the diffusion equation is $\nabla^2 n(x, y) - n(x, y)/L_{\mathrm{nh}}^2 = 0$ as shown in Fig. 1. By the same method used in the previous section, the general solution can be expressed easily as follows;

$$n(x, y) = \sum_{n=1}^{\infty} B_n \exp(-K_{\mathrm{n}} x) \cdot \cos\left(\frac{(2n-1)\pi y}{2y_m}\right) \quad (7)$$

where

$$K_{\mathrm{n}} = \sqrt{\frac{1}{L_{\mathrm{nh}}^2} + \left(\frac{(2n-1)\pi}{2y_m}\right)^2}.$$

Retain the first term only because of the rapid exponential decay in (7). In the heavily-doped substrate L_{nh} is about 0.2 μm while y_m is typically around 40 μm or more, hence K_{n} can be approximated by $1/L_{\mathrm{nh}}$. Utilizing the boundary condition at $x = x_{\mathrm{e}}^+$,

$$n(x, y)|_{x = x_{\mathrm{e}}^+} = B_1 \exp\left(-\frac{x_{\mathrm{e}}^+}{L_{\mathrm{nh}}}\right) \cdot \cos\left(\frac{\pi y}{2y_m}\right),$$

we obtain the following equation;

$$n(x, y) = n(x_{\mathrm{e}}^+, y) \exp\left(\frac{x_{\mathrm{e}}^+ - x}{L_{\mathrm{nh}}}\right). \quad (8)$$

With the boundary condition at $x = x_{\mathrm{e}}^+$, i.e., $J_{\mathrm{sub}}|_{x = x_{\mathrm{e}}^+} = qS_{pp^+}(n(x_{\mathrm{e}}^-, y) - n_0)$ and the relation in [9], i.e.,

$$\frac{n(x_{\mathrm{e}}^+, y)}{n(x_{\mathrm{e}}^-, y)} = \frac{N_{\mathrm{al}}^- + n(x_{\mathrm{e}}^-, y)}{N_{\mathrm{ah}}} \exp\left(\frac{\Delta E_{\mathrm{g}}}{KT}\right),$$

the magnitude of the surface recombination velocity can be derived as;

$$S_{pp^+} \cong \frac{D_{\mathrm{nh}}}{L_{\mathrm{nh}}} \exp\left(\frac{\Delta E_{\mathrm{g}}}{KT}\right) \frac{N_{al}}{N_{\mathrm{ah}}} \quad (9)$$

The following two arguments are used in the final step to (9): the minority carrier concentration is much less than the epitaxial-layer doping and the electric field usually ionize the acceptor impurity fully beneath the outer guard ring as indicated by the simulations. This final form, which is similar to that in [11], is independent of the Y-coordinates.

4. RESULTS AND DISCUSSIONS

In order to calculate the numerical values of the escape current, the temperature dependencies of the physical parameters used in the model should be clarified in advance. The forms of these quantities at RT were utilized mostly from [9]. Then the low-temperature values were calculated by their temperature dependencies respectively. In heavily-doped semiconductor, i.e., doping around $10^{18}\,\mathrm{cm}^{-3}$, the minority carrier mobility is nearly constant in the whole temperature range, so the diffusion constant becomes approximately $D_{\mathrm{nh}} \cong \mu(KT/q) \propto T$. The temperature dependence of the SRH recombination lifetime is adopted from [13] and the diffusion length is expressed as

$$L_{\mathrm{nh}} = \sqrt{D_{\mathrm{nh}}\tau_{\mathrm{nh}}} \propto \sqrt{T \cdot \frac{1}{T^{3/2}}} \propto T^{-1/4}.$$

In contrast, in the lightly-doped semiconductor the diffusion constant $D_{\mathrm{nl}} = \mu(KT/q) \propto T^{-3/2} \cdot T \propto T^{-1/2}$ because of dominant lattice scattering of carrier mobility from 300 K to about 50 K. As for the energy bandgap narrowing, there was no general agreement about the experimental data and also no sufficient model giving reliable predictions. The experimental values of the bandgap narrowing at low temperature scatter even wider and more incomplete[12,14]. Their accuracies which were at least 10 meV were not strict enough either. Hence the values used in the fitting processes are just approximations to those reported in [12] where temperature range concerned is only above 100 K.

Figure 3 shows the model calculations compared with the experimental data in [8]. A good agreement between the two was reached. The doping levels of the heavily-doped substrate and lightly-doped epitaxial-layer are 3.6×10^{18} and $2 \times 10^{15}\,\mathrm{cm}^{-3}$, respectively. The bandgap narrowing value is 59 meV. The fitted L_{eff} values at 77 K are 2.86 μm for 1.8 V and 2.32 μm for 1.4 V V_{be} biases. They are about

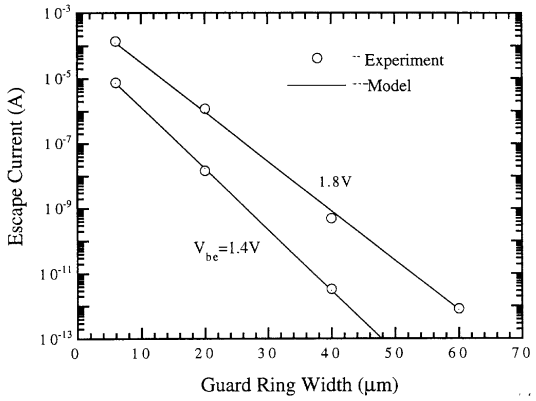

Fig. 3. The comparison between the model calculations and the experimental data at 77 K with epitaxial-layer thickness of 6 μm with the V_{be} bias of 1.4 and 1.8 V.

77% and 64% of the L_{eff} at RT. It is worth mentioning that the negative slope coefficient at 77 K becomes lessened with the applied V_{be} bias because of the more severe high injection condition. In the model fitting we have adjusted ξ to account for this tendency. The ξ value can be extracted from the exponential slope in log scale. According to experiment fitting results, the high-level injection parameter ξ value varies from very nearly 1 to about 2 as V_{be} increase from low to higher bias. However, n^* value ranges over one order of magnitude from about 10^{15} to 10^{16} cm^{-3}. n^* increases with respect to the increase of the epitaxial layer thickness and/or V_{be} bias. As compared with simulation results, the n^* value with a thinner epitaxial layer increases from 10^9 to 10^{14} cm^{-3} with the increase of V_{be} bias from slightly larger than 1 V to almost 2 V. From this result the feasibility of the model has verified favorably. It is not only available in low-temperature characteristics but also suitable for RT, applications in which surface recombination of the high/low junction cannot be negligible.

From (6) several implications can be obtained as well. According to the previous discussions in the physical parameters, the temperature dependence of the surface recombination velocity can be approximately expressed as;

$$S_{pp^+} \propto T^{5/4} \exp\left(\frac{\Delta E_g}{KT}\right)$$

and hence the temperature dependence of the escape current is roughly expressed as;

$$I_{esc} \propto \exp\left(-\sqrt{a + bT \cdot \exp\left(\frac{\Delta E_g}{KT}\right)}\right)$$

which is indeed a significant function of temperature. Moreover, the epitaxial-layer thickness term $(x_e - x_j)$ represents that the minority carriers are ideally confined in the sandwich layer while the surface recombination velocity S_{pp^+} indicates the sinking capability of the heavily-doped substrate. In (6) the epitaxial-layer thickness plays a more prominent role than the surface recombination velocity does because S_{pp^+} term is only a square root parameter whereas $(x_e - x_j)$ term is an inversely proportional function in the exponential term, which is consistent with the results in [8]. In the extreme case with very thick epitaxial layer the exponential term of the escape current can be simplified as

$$\exp\left(-\sqrt{3\left(\frac{S_{pp^+}}{\xi D_{nl}(x_e - x_j)}\right)} W_g\right),$$

the roles of S_{pp^+} and $(x_e - x_j)$ become even. This also indicates that for very thick epitaxial-layer the heavily-doped substrate become more significant in sinking the escaping carriers. In contrast, the general situation is that the term

$$\frac{S_{pp^+}(x_e - x_j)}{\xi D_{nl}} \approx 1.$$

This normally shows the more effectiveness of $(x_e - x_j)$ over S_{pp^+}. In the case of RT, typically

$$\frac{S_{pp^+}(x_e - x_j)}{\xi D_{nl}} \ll 1,$$

(6) is changed into a form with $L_{eff} = (x_e - x_j)/\sqrt{3}$, which is almost identical with that at RT[5,6].

The difference between the first and second term in (4) is the ratio factor

$$\exp\left(\frac{2\pi W_g}{(x_e - x_j)}\right).$$

Substituting the parameter values of the test structure, the ratio factor of the first term to the second term is calculated to be about 300. Thus the single term approximation in the final solution is satisfied completely. As far as the simplification of $\cot[m(x_e - x_j)]$ is concerned, the first three terms instead of two were also taken into account in solving (2). The resulting formulation is nearly identical to (3) except the slightly different numerical constant. Thus, the two-term approximation in the cotangent function is a feasible way for the analytic derivation.

5. CONCLUSION

A compact model dealing with low temperature operation was derived for the minority-carrier well-type guard rings in the epitaxial CMOS structures. It should be useful for low-temperature applications as well as RT circumstances whenever the ideal assumptions for the simple formulation are not valid.

Acknowledgements—The authors would like to thank Mr Ping-Nan Tseng, Taiwan Semiconductor Manufacturing Company (TSMC), for fabricating the guard-ring test structures designed by ourselves.

[1]*Mosel/Vitelic Inc., Hsinchu 300, Taiwan*
[2]*Department of Electronics Engineering and Institute of Electronics, National Chiao-Tung University, Hsinchu 300, Taiwan*

CHIH-YAO HUANG[1]
MING-JER CHEN[2]

REFERENCES

1. Quinke, J., *Microelectron. Reliab.*, 1990, **30,** 105.
2. Troutman, R. R., *Latchup in CMOS Technology: the Problem and its Cures*, Kluwer Academic Publishers, Boston, 1986.
3. Troutman, R. R., *IEEE Electron Dev. Lett.*, 1983, **4,** 438.
4. Chen, M. J. and Wu, C. Y., *Solid-St. Electron.*, 1987, **30,** 879.
5. Chen, M. J., Huang, C. Y., Tseng, P. N., Tsai, N. S. and Wu, C. Y., *Proc. IEEE Custom Integrated Circuits Conf.*, 1991, 4.5.1.
6. Chen, M. J., Huang, C. Y. and Tseng, P. N., *IEE Proc. G Circuits Dev. Syst.*, 1993, **140,** 182.
7. Huang, C. Y. and Chen, M. J., *IEEE Trans. Electron Dev.*, 1994, **41,** 1806.
8. Huang, C. Y., Chen, M. J., Jeng, J. K. and Wu, C. Y., *IEEE Trans. Electron Dev.*, 1996, **43,** 2249.

9. Wu, C. Y., *Solid-St. Electron.*, 1980, **23,** 641.
10. Roulston, J. R., *Bipolar Semiconductor Devices*, McGraw-Hill, New York, 1994, pp. 75.
11. Hauser, J. R. and Dunbar, P. M., *Solid-St. Electron.*, 1975, **18,** 715.
12. Lanyon, H. P. D. and Tuft, R. A., *IEEE Trans. Electron Dev.*, 1979, **26,** 1014.
13. Schenk, A., *Solid-St. Electron.*, 1992, **35,** 1585.
14. Swirhum, S. E., Kane, D. E. and Swanson, R. M., *Tech. Dig. IEDM*, 1988, 298.